From macroscopic yield criteria to atomic stresses in polymer glasses

David MacNeill and Jörg Rottler*
Department of Physics and Astronomy, The University of British Columbia, 6224 Agricultural Road, Vancouver, British Columbia, Canada V6T 1Z1

(Received 29 September 2009; published 12 January 2010)

The relationship between macroscopic shear yield criteria and local stress distributions in deformed polymer glasses is investigated via molecular dynamics simulations on different scales of coarse-graining. Macroscopic shear stresses at the yield point obey a pressure-modified von Mises (pmvM) criterion for many different loading conditions and strain rates. Average local stresses in small volume elements obey the same yield criterion for volumes containing approx. 100 atoms or more. Qualitatively different behavior is observed on smaller scales: the average octahedral atomic shear stress has a simple linear relationship to hydrostatic pressure regardless of macroscopic stress state and failure mode. Local plastic events are identified through a threshold in the mean-squared nonaffine displacement and compared to the local stress state. We find that the pmvM criterion only predicts local yield events when stress and displacements are averaged over at least 100 atoms. By contrast, macroscopic shear yield criteria appear to lose their ability to predict plastic activity on the atomic scale.

DOI: 10.1103/PhysRevE.81.011804 PACS number(s): 61.25.H−, 81.05.Kf, 83.60.La, 83.10.Mj

I. INTRODUCTION

Glassy polymers have many desirable mechanical properties [1]. They exhibit a large elastic limit of a few percent strain, and their yield stresses range between 5% and 10% of their elastic modulus [2]. The development of a fundamental understanding of their mechanical behavior, however, still poses great challenges to experiment, theory and simulations [3]. The stress required to deform glassy polymers at constant strain rate typically rises past the elastic response to a maximum or yield stress, followed by strain softening [4]. The yield stress is a complicated function of experimental control parameters that include temperature, deformation rate, sample history, and loading condition [2,4]. It generally increases with increasing strain rate and decreasing temperature, and the amount of strain softening is sensitive to the degree of annealing and physical aging [5,6].

In engineering applications, it is of particular importance to predict the stress state in a polymer glass at yield. Since amorphous solids are isotropic, one expects that the loading condition at yield will depend only on invariants of the stress tensor σ_{ij}, namely, the first invariant or hydrostatic pressure $p=-(\sigma_{xx}+\sigma_{yy}+\sigma_{zz})/3$ and the second invariant or octahedral stress $\tau_{\mathrm{oct}}=[(\sigma_{xx}-\sigma_{yy})^2+(\sigma_{yy}-\sigma_{zz})^2+(\sigma_{zz}-\sigma_{xx})^2+6(\sigma_{xy}^2+\sigma_{yz}^2+\sigma_{xz}^2)]^{1/2}/3$. While the hydrostatic pressure relates to volume changes, the octahedral stress couples to shear deformations that leave the volume invariant. When failure occurs through shear, experiments on many polymers [7–10] as well as computer simulations [11,12] show that the octahedral stress at yield is well described by the pressure-modified von Mises (pmvM) yield criterion,

$$\tau_{\mathrm{oct}}^{y}=\tau_0+\alpha p. \tag{1}$$

In some formulations, τ_{oct} is replaced with the von Mises equivalent stress $\tau_e\equiv 3\tau_{\mathrm{oct}}/\sqrt{2}$. This condition is motivated by the idea that the elastic energy associated with shear deformation reaches a critical value at the yield point. The constant τ_0 denotes the yield stress at zero hydrostatic pressure. It varies greatly between materials and also depends on control parameters such as temperature and strain rate. The pressure-dependence of the yield stress enters through a term linear in pressure, which is reminiscent of static friction where the force required to initiate sliding is proportional to normal load. The friction coefficient α is close to 0.1 for most amorphous polymers and metals. A similar friction term appears in the closely related Mohr-Coloumb (MC) criterion, $\tau_{\mathrm{oct}}^{y}=\tau_0-\alpha\sigma_n$, where σ_n is the stress normal to a failure plane. The linear dependence on σ_n has been verified directly through molecular statics simulations of elementary shear transformations [13]. MC type behavior can be observed in geometries that promote localized failure, such as thin films [14], but bulk systems that remain isotropic up to the yield point can be expected to follow the pmvM criterion. Equation (1) constrains the possible combinations of principal stresses at yield to a yield surface, which has the form of a tapered cylinder. When the loading condition becomes triaxial, the mode of failure changes to cavitation and the pmvM criterion no longer applies.

Although amorphous solids are isotropic on macroscopic scales, particle dynamics on the atomic scale is spatially and temporally heterogeneous [15]. While small groups of atoms are highly mobile, other regions do not change appreciably over the same time scales. Local elastic constants vary rapidly on the nanoscale [16] and appear to be correlated with irreversible deformation [17,18]. While the macroscopic stress state of a polymer glass at yield obeys the pmvM criterion quite well, the relationship between first and second stress invariant may therefore be different on smaller scales. Additionally, the pmvM criterion provides a robust prediction for the macroscopic yield stress, but it is not clear if it is capable of predicting localized plastic events on the atomistic scale.

In this work, we explore the relationship between the macroscopic pmvM criterion and the local stress state as well

*jrottler@phas.ubc.ca

as local plasticity in polymer glasses. We perform molecular dynamics simulations under deformation at constant strain rate for many different loading conditions, and compute not only the resultant macroscopic stress, but also distributions of local stresses in smaller volume elements containing different numbers of atoms down to a single atom. Our work aims to answer two distinct, but related questions: (i) what is the distribution of local stresses in a system that has been strained to the macroscopic yield point, and how do they relate to the pmvM criterion? (ii) Can the pmvM criterion be used to predict localized plastic events? If so, on what scale? We will show that there is a distinct crossover in behavior at scales of about 100 atoms or less. While the pmvM criterion is obeyed on average for coarse-grained volume elements containing more than 100 atoms, all correlation to plastic deformation is lost at smaller scales. Although we are simulating a model polymer glass, we expect that the conclusions will also be relevant for monovalent amorphous solids such as mixtures of particles interacting via Lennard-Jones (LJ) or other short-range forces [19].

II. METHODS

We study amorphous plasticity through molecular dynamics simulations of a standard coarse-grained bead-spring model for linear polymers [20–22]. Beads are bonded via a finite extensible nonlinear elastic (FENE) spring, and van der Waals forces between the beads are modeled with a truncated 6–12 Lennard-Jones potential,

$$V_{\mathrm{LJ}}(r) = 4\epsilon\left[\left(\frac{\sigma}{r}\right)^{12} - \left(\frac{\sigma}{r}\right)^{6}\right] \quad \text{for } r < r_c. \tag{2}$$

The parameters of the LJ potential σ and ϵ define a reference length and energy scale. These imply a reference time scale $\tau_{\mathrm{LJ}} = \sqrt{m\sigma^2/\epsilon}$, and we use $r_c = 1.5\sigma$. All simulations here use 4000 chains of 10 beads each in a cubic box subject to periodic boundary conditions, which is large enough to avoid finite size effects in the macroscopic mechanical response [23].

Unentangled polymer melts are created through a random walk procedure followed by a soft push-off phase to avoid particle overlap. The system is equilibrated at a melt temperature $T = 1.2\epsilon/k_B$ before undergoing a rapid quench into the glassy state at $T = 0.1\epsilon/k_B$. The initially cubic simulation box has $\tau_{\mathrm{oct}} = p = 0$ and is deformed at constant true strain rates $\dot{\epsilon}_i$. A broad range of loading conditions ranging from pure shear to isotropic tensile loading are realized by imposing different strain rates in different Cartesian directions as indicated in Table I. Unless otherwise stated, all strain rates are on order $10^{-5}/\tau_{\mathrm{LJ}}$.

It is convenient to quantify deformation in terms of an effective strain

$$\epsilon_{\mathrm{eff}} = \frac{1}{\sqrt{2}}[(\epsilon_{xx} - \epsilon_{yy})^2 + (\epsilon_{yy} - \epsilon_{zz})^2 + (\epsilon_{zz} - \epsilon_{xx})^2]^{1/2}. \tag{3}$$

The macroscopic stress tensor is computed from the usual virial expression,

TABLE I. Summary of loading conditions used in the present study. Strain rates are given in units of $10^{-5}\tau_{\mathrm{LJ}}^{-1}$, while p^y and τ_{oct}^y are given in units of ϵ/σ^3.

No.	$\dot{\epsilon}_{xx}$	$\dot{\epsilon}_{yy}$	$\dot{\epsilon}_{zz}$	p^y	τ_{oct}^y
1	1.5	2.0	0.0	−1.8707	0.1427
2	1.5	2.0	−0.3	−1.8478	0.1730
3	−0.5	1.5	1.0	−1.8510	0.2135
4	−0.5	1.5	0.8	−1.6377	0.2328
5	2.5	−0.5	−1.0	−0.7948	0.3486
6	−0.35	1.4	0.8	−1.6313	0.2079
7	2.0	2.0	2.0	−2.1839	0.0077
8	2.5	1.2	−1.7	−1.1229	0.3017
9	2.9	−1.0	−1.0	−0.5561	0.3605
10	1.0	1.0	−2.0	0.12	0.4051
11	1.1	−2.3	1.6	−0.2356	0.4109
12	1.0	1.0	−3.0	1.6635	0.5414
13	2.5	0.5	1.6	−2.0129	0.1179
14	−0.5	1.5	0.9	−1.6845	0.2261
15	2.2	1.55	−1.25	−1.4048	0.2713
16	2.5	−0.4	−0.9	−0.8769	0.3246
17	1.0	1.0	−2.4	0.7287	0.4841
18	−0.3	−1.0	2.5	−1.1084	0.3419
19	−0.8	3.2	−0.9	−0.9123	0.3316
20	1.2	2.4	−2.0	−0.9134	0.3274
21	1.0	1.0	−3.1	2.2325	0.5789

$$\sigma_{ij} = -\frac{1}{2V}\left(\sum_n m_n v_i^n v_j^n + \sum_n \sum_{m\neq n} r_i^{nm} F_j^{nm}\right). \tag{4}$$

Here, m_n and v_i^n denote the mass and velocity component of particle n, while F_i^{nm} denotes the i-component of the force acting between particles n and m separated by a distance r_i^{nm}, and V is the simulation box volume.

A similar expression can used to define an atomic stress tensor for atom m [24].

$$\sigma_{ij}^m = -\frac{1}{2v_m}\left(m_m v_i^m v_j^m + \sum_{n\neq m} r_i^{nm} F_j^{nm}\right). \tag{5}$$

Equation (5) has been applied multiple times to both polymer glasses [25,26] and amorphous metals [27]. In order to convert the virial into a stress, a local volume v_m has to be associated with each atom. Here, we shall use a Voronoi tessellation to define atomic volumes [28]. The macroscopic stress then follows from a weighted average:

$$\sigma_{ij} = \frac{1}{\sum_m v_m}\sum_m v_m \sigma_{ij}^m, \tag{6}$$

where it is understood that $\Sigma_m v_m = V$.

In addition to the atomic stress, we wish to obtain coarse-grained local stresses on different scales to examine the crossover to macroscopic behavior. There are several possibilities to compute the stress tensor in amorphous materials

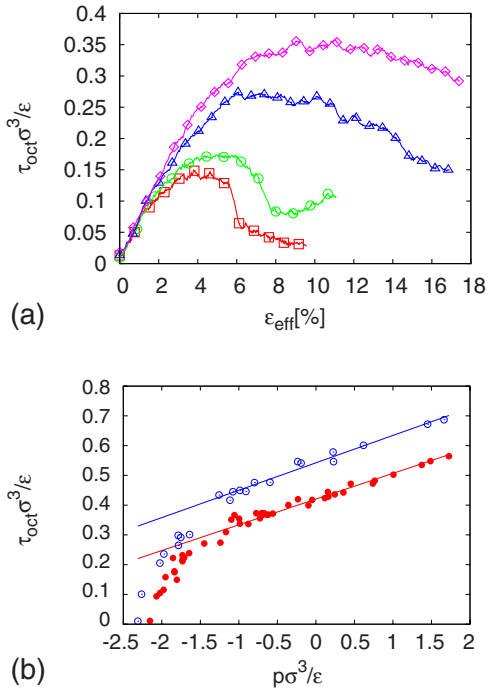

FIG. 1. (Color online) (a) Stress-strain curves of the polymer glass for loading conditions #1 (□), #2 (○), #15 (△), and #5 (◇) as indicated in Table I. (b) Octahedral stress vs pressure at yield for all loading conditions indicated in Table I as well as additional combinations with strain rates of order $10^{-5}/\tau_{LJ}$ (●). Also shown are yield stresses from similar loading conditions with higher strain rates on order $10^{-4}/\tau_{LJ}$ (○). Straight lines show fits to Eq. (1) with constants $\tau_0=0.41\epsilon/\sigma^3$, $\alpha=0.086$ (red, lower curve) and $\tau_0=0.54\epsilon/\sigma^3$, $\alpha=0.092$ (blue, upper curve).

on intermediate scales. Goldhirsch and Goldenberg suggest to introduce a coarse-graining function, e.g., a Gaussian, which smoothes the kinetic and virial contributions over the desired length scale [29]. Another popular approach has been to partition the simulation cell into subvolumes, and only those atoms residing in that volume contribute to the local stress tensor of the region [16]. To avoid artificial discontinuities from atoms crossing boundaries, individual contributions in the virial stress are weighted with the fraction of the bond r_i^{nm} lying inside the averaging volume [30,31]. Here, we pursue a similar approach and subdivide our simulation cell into 8, 64, 512, and 4096 rectangular bins containing approximately 5000, 625, 78, and 10 atoms, respectively. The stress tensor within a bin is computed according to Eq. (6), where the sum runs only over those atoms that are in the given bin at a particular time. This implies that the bin volumes $V_{bin}=\Sigma_m v_m$, and number of atoms per bin are not all equal but fluctuate slightly depending on the local particle density and shape of the simulation cell. This scheme converges to the macroscopic stress Eq. (4) when the simulation box is taken as a single bin.

III. RESULTS

Typical simulated stress-strain curves resulting from deformation of our polymer glass model are show in Fig. 1(a).

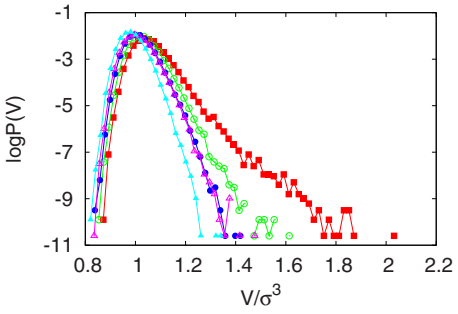

FIG. 2. (Color online) Distribution of Voronoi volumes at the yield point for loading conditions #7 (■, pure cavitational failure), #4 (○), #8 (●), #9 (△), and #11 (▲, pure shear failure) as indicated in Table I.

One can see that the octahedral shear stress peaks at yield strains between 5% and 10%, and we define the maximum of τ_{oct} as the yield stress τ_{oct}^y and denote the corresponding pressure at yield with p^y. As the failure mode changes from shear (upper curves) to cavitation (lower curves), the octahedral stress decreases but the stress drop following yield becomes more pronounced.

Figure 1(b) plots τ_{oct}^y as a function of pressure p^y at yield from these stress-strain curves as well as many more loading conditions. Most data points fall along a straight line as predicted by Eq. (1). At $p\approx-1.7\epsilon/\sigma^3$, the data points sharply deviate from the von Mises line, signaling a change in failure mode from shear yielding to cavitation. The pmvM criterion only describes volume conserving shear and is expected to fail when the dilational component of the deformation increases. These results confirm those obtained in Ref. [11] for a very similar polymer model. Here, we also show a data set obtained at higher strain rates. Both shear and cavitational yield stresses increase and the crossover to cavitation occurs at slightly higher pressures, but again most data points obey the pmvM criterion. Note that the cavitational yield stress is less sensitive to strain rate than the shear yield stress, while the value of the friction constant α is independent of rate.

The difference in behavior for shear yielding and cavitation can be nicely observed as a change in the distributions of Voronoi volume at the yield point, which are shown in Fig. 2. Three of these curves correspond to pure shear failure, one curve to pure cavitation, and one curve was taken right at the crossover between the failure modes. All distributions are centered at $1\sigma^3$ and have a Gaussian shoulder on the small volume side, but exhibit an exponential tail for large volumes. The slope of the exponential tail starts to decrease right at the point where the mode of failure changes from shear to cavitation, reflecting the dilational component of the deformation and the formation of microvoids.

A. Local stress distributions at macroscopic yield

We now proceed to analyze the distributions $P(\tau_{oct})$ and $P(p)$ of octahedral shear stress and pressure at different levels of coarse-graining when the system has been strained to the macroscopic yield point. Inspecting first the atomic level stresses, we see in Figs. 3(a) and 3(b) that while the pressure

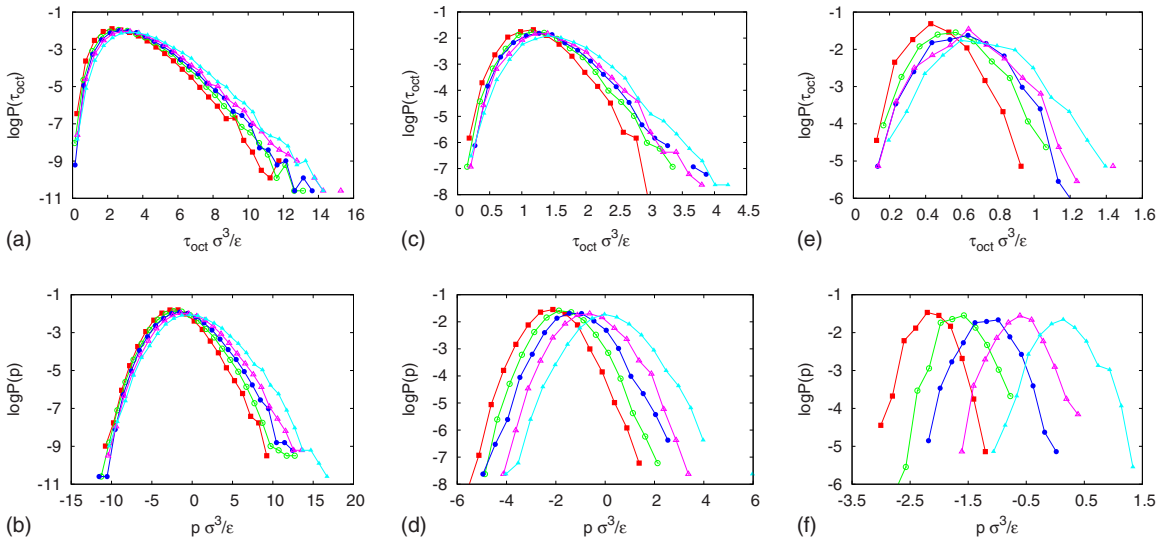

FIG. 3. (Color online) Distributions of pressure $P(p)$ and octahedral stress $P(\tau_{\mathrm{oct}})$ at yield at the atomic level (a,b) as well as in bins containing approximately 10 (c,d) and 78 atoms (e,f), respectively. Symbols correspond to loading states as indicated in Fig. 2.

distributions are almost symmetrically centered around the macroscopic pressure, the distributions of τ_{oct} are highly skewed and exhibit large fluctuations with an exponential tail. Such behavior is typical for amorphous solids [25]. As failure shifts from shear to cavitation, both distributions narrow and the pressure distribution shift toward negative pressure. Very similar behavior is found on the first level of coarse-graining, where bins contain about 10 atoms, see Figs. 3(c) and 3(d). The magnitude of the stresses decreases, but the τ_{oct}-distributions are still notably skewed. When the bin size is increased again so that the stresses are averaged over about 78 atoms, however, one can see in Fig. 3(e) that the distributions become much more symmetric and the size of the fluctuations is greatly reduced. Similarly, the pressure distributions now take the form of near perfect Gaussians whose mean shifts again toward negative tensile pressure for cavitational failure.

In order to determine whether the macroscopic pmvM criterion also determines the local stress state in a polymer glass at yield, we compute the average octahedral shear stress from the distributions in Fig. 3 and plot the result against the average pressure in Fig. 4 for all levels of coarse-graining and for all loading conditions. Also shown is the macroscopic yield stress data from Fig. 1(b). Data for each scale fall along a straight line and can therefore be fit to Eq. (1). Data for macroscopic yield and bins containing 5000 and 625 particles collapse on top of each other. Deviations from the bulk pmvM behavior start to appear at the next smaller coarse-graining scale that averages over 78 atoms. The friction coefficient α in the pmvM law is still almost unchanged, but the offset τ_0 has increased, reflecting the increasing magnitude of the local shear stresses. On a scale of one and 10 atoms, both α and τ_0 have increased significantly and deviate from the macroscopic values. We conclude that although the average local octahedral shear stress obeys the functional form of the pmvM criterion, there is a change in behavior when the stresses are averaged over 78 atoms or less.

As an alternative analysis of the behavior of local stresses at yield, we consider in Fig. 5 scatter plots of local values of τ_{oct} in bins at 5 different levels of coarse-graining for many loading conditions. In this representation, it is particularly easy to observe the increasing amount of fluctuations as the coarse-graining scale decreases. At all scales, however, there is a clear positive correlation between shear stress and pressure. Linear fits to the scatter data capture this trend rather well, and the resulting coefficients are compared to those obtained from the correlation between $\langle\tau_{\mathrm{oct}}\rangle$ and pressure in Table II. We find excellent overall agreement between the two data sets. Analysis of the scatter plots shows again that the friction coefficient $\alpha \approx 0.09$ from the macroscopic value to 78 atoms/bin, but then starts to increase. Similarly, the offset $\tau_0 \approx 0.4\epsilon/\sigma^3$ on the three coarsest levels, but then increases to $\tau_0 \approx 3.9\epsilon/\sigma^3$.

Although the functional form of the pmvM criterion appears to hold *on average* at all scales of coarse-graining, the increase in fluctuations casts doubt on its physical significance. The pmvM condition constrains the possible principal stress combinations, and it is instructive to ask whether this condition holds only at yield or more generally. To this end, we show in Fig. 6 parametric plots of $\langle\tau_{\mathrm{oct}}\rangle$ vs pressure for a range of deformations at different strains between zero and

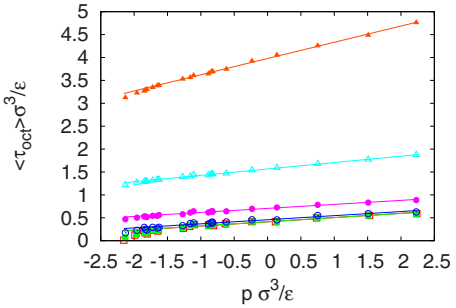

FIG. 4. (Color online) Average octahedral stress $\langle\tau_{\mathrm{oct}}\rangle$ at the macroscopic yield point for the atomic stress (▲) and averaged within bins containing 10 (△), 78 (●), 625 (○), and 5000 (■) atoms and the macroscopic yield stress (□). Solid lines are fits to Eq. (1) and the coefficients τ_0^{av} and α_{av} are reported in Table II.

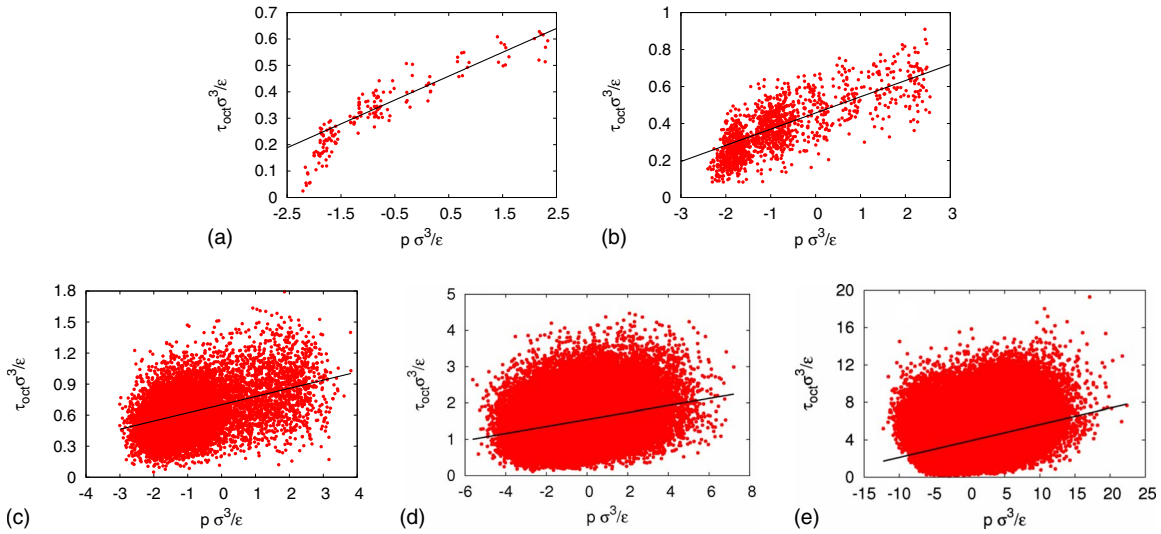

FIG. 5. (Color online) Scatter plots of octahedral stresses at yield vs pressure. The bins contained approximately (a) 5000, (b) 625, (c) 78, and (d) 10 atoms, and (e) shows the atomic stress. Solid lines are fits to Eq. (1) and the coefficients τ_0 and α are reported in Table II.

the yield strain. One can see in Fig. 6(a) that in bins containing 5000 atoms, the pmvM condition is only fulfilled when the system reaches the yield point, and the pmvM line appears as an envelope to the individual loading curves. At the next two smaller levels of coarse-graining, 625 and 78 atoms/bin, this behavior persists but becomes gradually reduced. Remarkably, for 10 atoms/bin and the atomic stress, we find that all data points fall onto a straight line regardless of loading state. Note in particular that this includes the data points belonging to cavitational failure, which strongly deviate from the pmvM line for macroscopic stress. It appears that in amorphous packings such as our polymer glass, atomic stresses obey a pmvM like constraint, $\langle \tau_{oct} \rangle = \tau_0^{av} + \alpha^{av} p$, at all times and not only at macroscopic yield. During deformation, different combinations of p and $\langle \tau_{oct} \rangle$ are realized along the von Mises line, but these do not carry any specific information about the macroscopic yield state or the mode of failure.

B. pmvM criterion and local plastic events

The data from Fig. 6 show clearly that *average* atomic stresses satisfy the functional form of the pmvM criterion trivially at all times. It is not clear yet, however, whether there exists a correlation between the local stress state and the occurrence of local plastic rearrangements. Previous work has shown that irreversible deformation in polymer glasses occurs long before the macroscopic shear stress reaches a maximum [11,26]. A frequently used measure of local plastic activity in amorphous packings is the nonaffine displacement of particle i [32–35],

$$\Delta r_{i\alpha}^{na} = r_{i\alpha} - r_{i\alpha}^0 - \epsilon_{\alpha\beta} r_{i\beta}^0, \tag{7}$$

where $\mathbf{r}_i^0$ denotes the particle position at a reference time and $\epsilon_{\alpha\beta}$ is the macroscopic strain tensor. In the following discussion, the reference state is always the unstrained solid at the beginning of the deformation.

To illustrate the evolution of this quantity during deformation, we show in Fig. 7 the mean-squared nonaffine displacement $\langle (\Delta r^{na})^2 \rangle$ for several deformations that include shear and cavitation. One can see that for shear yielding, $\langle (\Delta r^{na})^2 \rangle$ rises continuously without any characteristic feature indicating global yield. The onset of cavitation, however, is extremely well signaled through a divergence at about 5% strain.

In order to use $\langle (\Delta r^{na})^2 \rangle$ as a diagnostic for plasticity, it is, therefore, necessary to associate yield with an (arbitrary) threshold. A suitable range for possible values of this threshold can be obtained from Fig. 8(a), which shows the value of $\langle (\Delta r^{na})^2 \rangle$ at the macroscopic yield point for a range of loading conditions. We find that $\langle (\Delta r^{na})^2 \rangle$ ranges between 0.05 and 0.15 σ^2, with the smallest values occurring for cavitational failure. In the following, we shall therefore use 0.1 σ^2 as a typical value of $\langle (\Delta r^{na})^2 \rangle$ at yield [36]. Figure 8(b) shows that this threshold, when applied to the mean-squared nonaffine displacement, would predict yield strains that only slightly overestimate those obtained from the maximum shear stress definition of yielding.

Having defined a yield threshold, we now analyze the dynamics of yielding at different levels of coarse-graining. First, we examine the number of yield events per unit time

TABLE II. Coefficients α^{av} and τ_0^{av} from fits of the data in Fig. 4 to Eq. (1) and coefficients α and τ_0 from the corresponding fits to the scatter plots in Fig. 5.

Atoms/bin	α^{av}	τ_0^{av}	α	τ_0
40000	0.093	0.41	0.093	0.41
5000	0.090	0.41	0.09	0.41
625	0.089	0.46	0.088	0.46
78	0.088	0.71	0.080	0.70
10	0.14	1.57	0.096	1.54
1	0.355	3.98	0.176	3.87

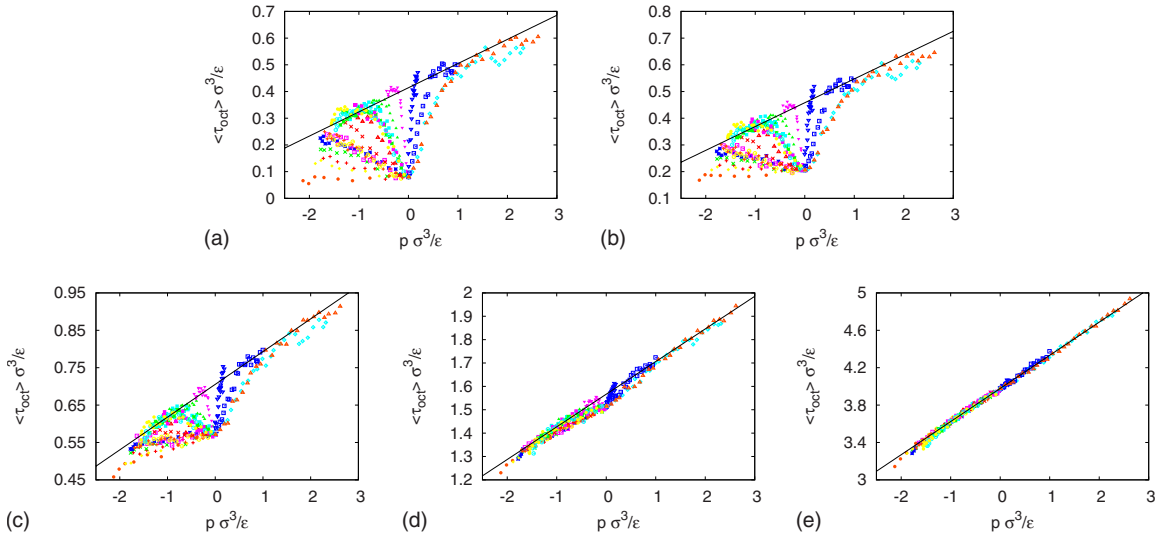

FIG. 6. (Color online) Parametric plot of $\langle \tau_{oct} \rangle$ against pressure for strains between zero and the yield strain. The bins contained approximately (a) 5000, (b) 625, (c) 78, and (d) 10 atoms, and (e) shows the average atomic stress. Solid lines are the fit lines obtained in Fig. 4.

for two typical deformations representative of shear and cavitational failure in Figs. 9(a) and 9(b). Yield is defined to occur in a bin when $\langle (\Delta r^{na})^2 \rangle_{bin} = 0.1\sigma^2$. Here, the average is taken over particles in a particular bin, and we only consider the first yield event for every bin. At all levels of resolution, the yield rate reaches a maximum at the same time, which coincides with the time it takes to strain to yield. The distributions broaden as the bins become smaller, which indicates that many single atoms reach the above defined yield threshold a long time before the system reaches macroscopic yield. Clearly, an accumulation of many local plastic events forms the total response of the system. This effect can be seen even more clearly in Figs. 9(c) and 9(d), which plots the cumulative distributions or fraction of bins that have undergone yield at a given time. While this fraction jumps discontinuously from zero to one for the total system, the saturation becomes much smoother with decreasing bin size and takes longer for shear yielding than for cavitation.

A direct test whether the pmvM criterion is capable of predicting local plastic events consists in examining the stress state of volume elements that have just experienced yield. If the pmvM criterion holds, one expects a linear relationship between octahedral shear stress and pressure. According to Fig. 10(a), this is indeed the case on the macroscopic level: values of τ_{oct} at times where $\langle (\Delta r^{na})^2 \rangle = 0.1$ collapse on a straight line when plotted against pressure, and deviate at negative pressure when cavitation sets in. The values also agree perfectly with the maximum shear stress τ_{oct}^{y}, even though the nonaffine threshold criterion predicts yield at slightly different times. This effect can be understood from Fig. 6(a), where one can see that the combinations of τ_{oct} and p satisfying the pmvM criterion occur not only strictly at yield but within a finite time interval following yield. The ability of the pmvM to predict plasticity continues to hold for bins containing 5000 and 625 atoms, see Fig. 10(b) and 10(c). Although the scatter of the data increases, the octahedral shear stresses at yield agree well with those stresses determined from the maximum shear stress definition (see also Figs. 1 and 5). For bins containing 78 atoms, we can still identify a linear trend, but the scatter has increased significantly. Data for the two smallest levels of coarse-graining are also shown in Figs. 10(e) and 10(f), but since the average atomic stresses already satisfy the pmvM equation at all times, we expect to recover this trend in the scatter plot.

The above results suggest that the stress state in yielding bins follows a pmvM law for 625 atoms/bin and above, but

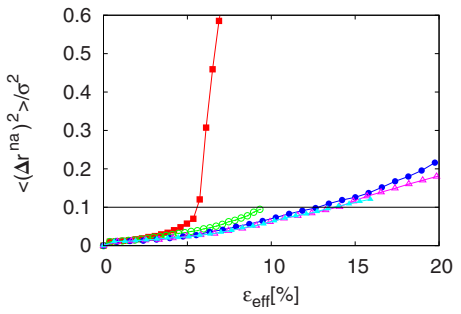

FIG. 7. (Color online) Average atomic nonaffine displacements $\langle (\Delta r^{na})^2 \rangle$ as a function of effective strain for several different deformations. The yield stresses for these runs are $\tau_{oct}^{y} = 0.11$ (■), 0.24 (○), 0.31 (●), 0.37 (△), and 0.41 (▲). The average was taken over all atoms in the simulation box.

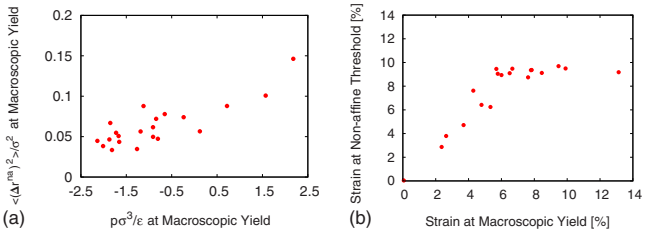

FIG. 8. (Color online) (a) $\langle (\Delta r^{na})^2 \rangle$ at yield as a function of pressure at yield for different deformations. (b) Strain for $\langle (\Delta r^{na})^2 \rangle$ to reach a threshold on 0.1 σ^2 vs strain to reach macroscopic yield.

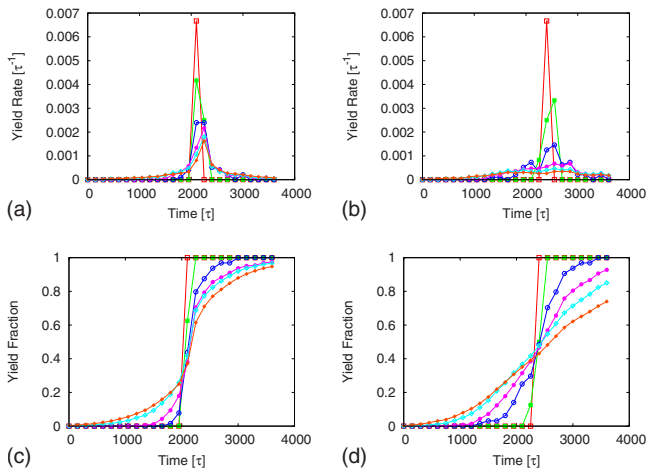

FIG. 9. (Color online) Yield rates and fraction of bins that have undergone a yield event for (a,c) caviation and (b,d) shear yielding. The bins contained 1 (♦), 10 (◇), 78 (●), 625 (○), 5000 (■), and 40000 atoms (□).

starts to cross over into new behavior for smaller volume elements. The significance of the correlations found in Fig. 10 can be tested by plotting combinations of τ_{oct} and p at random times during the straining interval. From Figs. 11(a)–11(c), it is evident that the good correlation between shear stress at yield and the pmvM condition is lost. For the two smallest bin sizes [Figs. 11(e) and 11(f)], there is no discernible difference between stresses plotted at random and at yield, and the bin size containing 78 atoms appears to be showing crossover behavior between the two limits [(Fig. 11(d)]. A more quantitative view can be taken by comparing the best fits of Eq. (1) to the two data sets in Table III. Here, we see that there are systematic discrepancies between the stresses at yield times vs random times for the largest bin sizes, but we obtain statistically identical results for 10 atoms/bin as well as the atomic stresses. To further confirm that the crossover scale to obtain pmvM like behavior is on the order 100 atoms, we associate a coarse-grained stress directly with each atom by averaging over contributions from all neighboring atoms located in rectangular bins centered on each atom. For bin sizes containing approx. 78 atoms, the resulting τ_{oct} and p-correlations now agree very well with those obtained from fixed bins of the same size.

IV. SUMMARY AND DISCUSSION

The identification of a local order parameter that predicts time and place of elementary shear transformations in amorphous solids is a prerequisite for the first-principles development of plasticity models. In this study, we examined the connection between macroscopic yield, local stress states and local plastic activity on several different length scales. In accord with previous simulations and the experimentally observed yield behavior of many polymers, the pmvM criterion accurately describes the principal stress combinations at the macroscopic yield point (maximum octahedral shear stress). We then partitioned the simulation cell into smaller volume elements and computed the distribution of local octahedral shear stresses and pressures down to the atomic level. Although fluctuations increase with decreasing coarse-graining scale, we found that the macroscopic pmvM expression continues to hold with the same parameters for the *average* stresses in bins containing about 100 atoms or more only at the macroscopic yield point. For bins containing only one or 10 atoms, however, we found qualitatively different behavior: octahedral atomic stress and pressure are always linearly related regardless of macroscopic loading state. It appears that this is a general feature of amorphous packings [25].

The crossover between atomistic and bulk behavior at about 100 atoms corresponds to a length scale of 4 and 5 particle diameters, which reaches beyond the second peak of

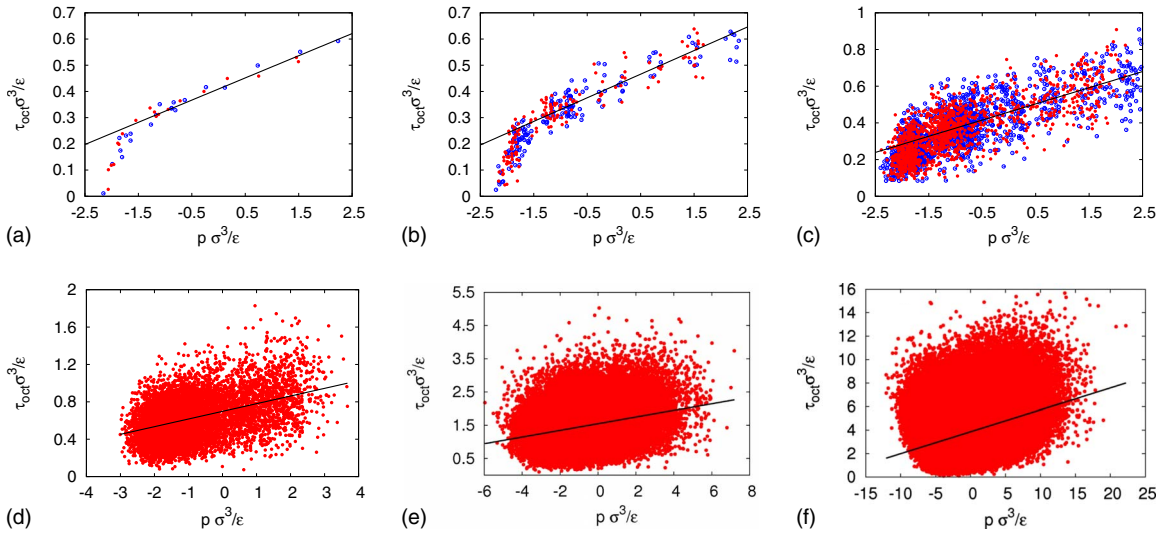

FIG. 10. (Color online) Scatter plot of octahedral shear stress vs pressure in bins that have reached the yield threshold $\langle(\Delta r^{\mathrm{na}})^2\rangle_{\mathrm{bin}}=0.1\sigma^2$ (red, solid symbols). The bins contained approximately (a) 40000, (b) 5000, (c) 625, (d) 78, and (e) 10 atoms, and (f) shows the atomic stress. Also shown (blue, open symbols) in (a–c) are the maximum octahedral stresses and corresponding pressures. Solid lines are fits to Eq. (1) and the coefficients τ_0^{na} and α^{na} are reported in Table III.

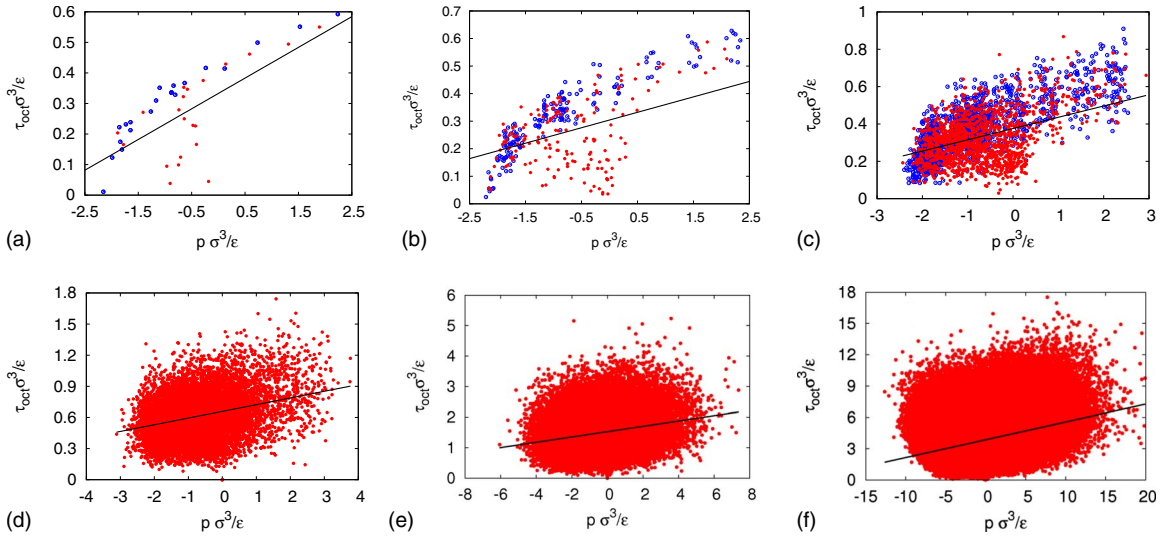

FIG. 11. (Color online) Scatter plot of octahedral shear stress vs pressure in bins at random times (red, solid symbols). The bins contained approx. (a) 40000 (b) 5000, (c) 625, (d) 78, and (e) 10 atoms, and (f) shows the atomic stress. Also shown (blue, open symbols) in (a)–(c) are the maximum octahedral stresses and corresponding pressures. Solid lines are fits to Eq. (1) and the coefficients τ_0^{rand} and α^{rand} are reported in Table III.

the static structure factor. It is interesting to note that in a recent study of local elastic properties in an athermal two-dimensional (2D) polydisperse Lennard-Jones mixture, a very similar coarse-graining scale of about 5 σ was identified below which Hooke's law is no longer valid [18]. Above this scale, elastic properties are heterogeneous and average out to homogeneous behavior on scales of approximately 20 σ. Since the von Mises yield criterion is motivated by the idea that the elastic energy associated with shear deformation reaches a critical value at yield, it is perhaps not surprising that its loss of validity coincides with that of linear elasticity. The similar crossover length scales may be due to the fact that the low strain behavior of the two models is similar [37]. The precise value of crossover length is likely not universal and may be different in fully atomistic polymer models that include angle and dihedral terms.

We also investigated the local significance of the pmvM condition by computing stress states at times when the local mean-squared nonaffine displacement reaches a threshold value. The nonaffine displacement had been shown previously to be a very sensitive indicator of plastic activity. The combinations of τ_{oct} and p in the yielding bins do agree well with the pmvM condition on the coarsest scales up to 78 atoms. Since a pmvM like expression was found to hold on smaller scales regardless of deformation state, we conclude that the pmvM condition has no predictive power over plastic events on scales smaller than 100 atoms. Further support for this interpretation comes from a study of atomic stress distributions in a 2D Lennard-Jones amorphous solid under shear by Tsamados *et al.* [38]. In this work, individual plastic rearrangements of quadrupolar symmetry are identified in the nonaffine displacement, but no connection was found between the location of these events and the local atomic stress. The authors also conclude that global yield criteria do not provide a locally selective criterion for plasticity.

TABLE III. Coefficients from fits to Eq. (1). α^{na} and τ_0^{na} were obtained from the data in Fig. 10 and α^{rand} and τ_0^{rand} correspond to the data in Fig. 11.

Atoms/bin	α^{na}	τ_0^{na}	α^{rand}	τ_0^{rand}
40000	0.085	0.41	0.10	0.33
5000	0.090	0.42	0.056	0.30
625	0.088	0.46	0.06	0.38
78	0.082	0.70	0.06	0.65
10	0.10	1.54	0.087	1.53
1	0.186	3.86	0.17	3.86

The present findings have implications for the interpretation of the role of stress in deformed glassy solids. Viscosity and hence relaxation times are often assumed to decrease with applied stress σ by a factor $\sigma/\sinh[\sigma V/k_BT]$ [39], but experiments have revealed that the accelerated dynamics under load does not scale with true stress in this form and depends on other parameters as well [40]. Modified versions of such transition rates for elementary shear events are used in the Shear-Transformation-Zone (STZ) theory of plastic deformation [41,42]. Other approaches such as the Soft Glassy Rheology (SGR) model emphasize instead the role of local strain in the activated hopping dynamics of mesocopic elements [43]. The results here suggest that local stresses, unless coarse-grained over several particle diameters, bear little correlation with the occurrence of local plastic events. Further simulation work may help to clarify whether local stress or local strain is the better variable to describe structural relaxation and yield rates in amorphous solids.

ACKNOWLEDGMENTS

We thank the Natural Sciences and Engineering Research Council of Canada (NSERC) for financial support.

[1] I. M. Ward and J. Sweeney, *An Introduction to the Mechanical Properties of Solid Polymers* (Wiley, New York, 2004).
[2] R. N. Haward and R. J. Young, *The Physics of Glassy Polymers* (Chapman and Hall, London, 1997).
[3] H. E. H. Meijer and L. E. Govaert, Prog. Polym. Sci. **30**, 915 (2005).
[4] Z. H. Stachurski, Prog. Polym. Sci. **22**, 407 (1997).
[5] E. T. J. Klompen, T. A. P. Engels, L. E. Govaert, and H. E. H. Meijer, Macromolecules **38**, 6997 (2005).
[6] J. Rottler and M. O. Robbins, Phys. Rev. Lett. **95**, 225504 (2005).
[7] I. M. Ward, J. Mater. Sci. **6**, 1397 (1971).
[8] P. B. Bowden and J. A. Jukes, J. Mater. Sci. **7**, 52 (1972).
[9] R. Raghava, R. M. Caddell, and G. S. Y. Yeh, J. Mater. Sci. **8**, 225 (1973).
[10] R. Quinson, J. Perez, M. Rink, and A. Pavan, J. Mater. Sci. **32**, 1371 (1997).
[11] J. Rottler and M. O. Robbins, Phys. Rev. E **64**, 051801 (2001).
[12] B. Vorselaars, A. V. Lyulin, and M. A. J. Michels, J. Chem. Phys. **130**, 074905 (2009).
[13] C. A. Schuh and A. C. Lund, Nature Mater. **2**, 449 (2003).
[14] J. Rottler and M. O. Robbins, Comput. Phys. Commun. **169**, 177 (2005).
[15] M. D. Ediger, Annu. Rev. Phys. Chem. **51**, 99 (2000).
[16] K. Yoshimoto, T. S. Jain, K. Van Workum, P. F. Nealey, and J. J. de Pablo, Phys. Rev. Lett. **93**, 175501 (2004).
[17] G. J. Papakonstantopoulos, R. A. Riggleman, J.-L. Barrat, and J. J. de Pablo, Phys. Rev. E **77**, 041502 (2008).
[18] M. Tsamados, A. Tanguy, C. Goldenberg, and J.-L. Barrat, Phys. Rev. E **80**, 026112 (2009).
[19] C. E. Maloney and A. Lemaitre, Phys. Rev. E **74**, 016118 (2006).
[20] K. Kremer and G. S. Grest, J. Chem. Phys. **92**, 5057 (1990).
[21] C. Bennemann, W. Paul, K. Binder, and B. Dunweg, Phys. Rev. E **57**, 843 (1998).
[22] J. Baschnagel and F. Varnik, J. Phys.: Condens. Matter **17**, R851 (2005).
[23] R. A. Riggleman, H.-N. Lee, M. D. Ediger, and J. J. de Pablo, Phys. Rev. Lett. **99**, 215501 (2007).
[24] J. H. Irving and J. G. Kirkwood, J. Chem. Phys. **18**, 817 (1950).
[25] D. N. Theodorou and U. W. Suter, Macromolecules **19**, 379 (1986).
[26] P. H. Mott, A. S. Argon, and U. W. Suter, Philos. Mag. A **67**, 931 (1993).
[27] D. Srolovitz, V. Vitek, and T. Egami, Acta Metall. **31**, 335 (1983).
[28] http://math.lbl.gov/voro++/
[29] I. Goldhirsch and C. Goldenberg, Eur. Phys. J. E **9**, 245 (2002).
[30] J. F. Lutsko, J. Appl. Phys. **64**, 1152 (1988).
[31] J. Cormier, J. M. Rickman, and T. J. Delph, J. Appl. Phys. **89**, 99 (2001).
[32] A. Tanguy, F. Leonforte, and J.-L. Barrat, Eur. Phys. J. E **20**, 355 (2006).
[33] F. Leonforte, R. Boissiere, A. Tanguy, J. P. Wittmer, and J.-L. Barrat, Phys. Rev. B **72**, 224206 (2005).
[34] F. Leonforte, A. Tanguy, J. P. Wittmer, and J.-L. Barrat, Phys. Rev. B **70**, 014203 (2004).
[35] A. Tanguy, J. P. Wittmer, F. Leonforte, and J.-L. Barrat, Phys. Rev. B **66**, 174205 (2002).
[36] The findings in this section are not dependent on this particular value of the threshold: qualitatively similar results have also been obtained for other thresholds ranging between 0.1 and 0.2 σ^2.
[37] C. D. Lorenz and M. J. Stevens, Phys. Rev. E **68**, 021802 (2003).
[38] M. Tsamados, A. Tanguy, F. Léonforte, and J.-L. Barrat, Eur. Phys. J. E **26**, 283 (2008).
[39] H. Eyring, J. Chem. Phys. **4**, 283 (1936).
[40] H.-N. Lee, K. Paeng, S. F. Swallen, and M. D. Ediger, Science **323**, 231 (2009).
[41] M. L. Falk and J. S. Langer, Phys. Rev. E **57**, 7192 (1998).
[42] J. S. Langer, Phys. Rev. E **77**, 021502 (2008).
[43] P. Sollich, F. Lequeux, P. Hebraud, and M. E. Cates, Phys. Rev. Lett. **78**, 2020 (1997).